ISSN 1070-3632, Russian Journal of General Chemistry, 2013, Vol. 83, No. 12, pp. 2352–2360. © Pleiades Publishing, Ltd., 2013.

Synthesis, Experimental and DFT Studies on Crystal Structure, FT–IR, ^{1}H, and ^{13}C NMR Spectra, and Evaluation of Aromaticity of Three Derivatives of Xanthens[1]

L. Zare Fekri[a], M. Nikpassand[b], and M. Goldoost[a]

[a] *Department of Chemistry, Payame Noor University, PO Box 19395-3697 Tehran, Iran*
email: chem_zare@pnu.ac.ir; chem_zare@yahoo.com

[b] *Department of Chemistry, Rasht Branch, Islamic Azad University, Rasht, Iran*

Received July 22, 2013

Abstract—Several derivatives of xanthenes are prepared by the condensation of aldehydes and dimedone in H_2O in the presence of a catalytic amount of trichlorotriazine. The crystalline products were characterized by FTIR, ^{1}H, and ^{13}C NMR spectra. Density Functional Theory (DFT) calculations on the B3LYP level were used to optimize the geometry and calculate the crystal structure, FTIR, ^{1}H NMR and ^{13}C NMR spectra of the selected synthesized compounds. We found that the values of FTIR, ^{1}H, and ^{13}C NMR spectra obtained by the B3LYP method are in accordance with experimental data. The calculated NICS indicate that the six-membered rings in xanthenes are essentially homoaromatic.

DOI: 10.1134/S107036321312027X

INTRODUCTION

Xanthene derivatives are important heterocyclic compounds because of their useful biological and pharmacological properties like antiviral, antibacterial and antiinflammatory activities [1]. These compounds are also used as dyes [2], as luminescent sensors [3], in laser technologies [4], in fluorescent materials for the visualization of biomolecules [5], and in photodynamic therapy [6].

In recent years, density functional theory (DFT) calculations have been used extensively for calculating a wide variety of molecular properties such as equilibrium structure, charge distribution, FTIR and NMR spectra, and have provided reliable results which are in agreement with experimental data [7]. In this research, Beck's three-parameter exchange functional [8] with Lee, Yang and Parr's [9] correlation functional (B3LYP) developed by Truhlar et al. [10] have been used to perform theoretical calculations on the structure, FTIR, ^{1}H, and ^{13}C NMR spectra, and some additional properties of the title compounds.

In 1996, Schleyer [11] proposed the nucleus independent chemical shifts (NICS) as a reliable criterion of aromaticity. The nucleus independent chemical shift (NICS) calculated at the ring center is a good criterion for aromaticity in such molecules.

EXPERIMENTAL

IR spectra were determined on a Shimadzu IR-470 spectrometer. ^{1}H NMR spectra were obtained on a Bruker DRX 500, and ^{13}C NMR spectra, on a Bruker DRX 125 Avance spectrometer, in $CDCl_3$ as solvent and with TMS as internal reference. Chemicals were purchased from Merck and Fluka. All used solvents were dried and distilled according to standard procedures.

A mixture of aldehyde (1 mmol), dimedone (2 mmol), and 0.03 g of trichlorotriazine (TCT) in 10 mL of H_2O were refluxed for the required reaction time (2–6 min). The progress of the reaction was monitored by TLC (EtOAc:petroleum ether 1 : 4). After completion of the reaction, the mixture was filtered. The product was recrystallized from ethanol to produce xanthene derivatives **IIIa–IIIc** as pure crystalline products.

3,4,6,7-tetrahydro-9-(4-methoxyphenyl)-3,3,6,6-tetramethyl-2*H*-xanthene-1,8-(5*H*,9*H*)-dione (IIIa). Colorless solid; mp: 146–148°C; ^{1}H NMR (500 MHz, $CDCl_3$), δ, ppm: 0.99 s (6H); 1.1 s (6H); 2.2 q (J = 16.4 Hz, 4H); 2.45 s (4H); 3.73 s (3H); 4.7 s (^{1}H), 6.73 d (J = 8.62 Hz, 2H), 7.18 d (J = 8.6 Hz, 2H). ^{13}C NMR

[1] The text was submitted by the authors in English.

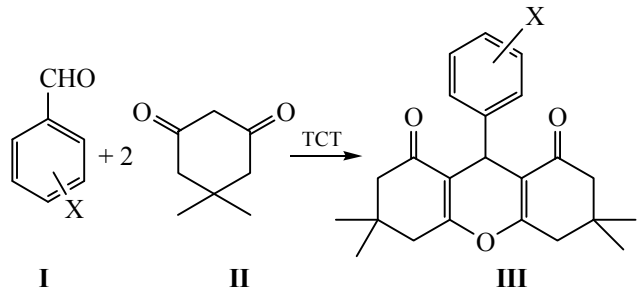

Scheme 1. Pathway to xanthenes synthesis.

Table 1. Effect of catalyst amount on the synthesis of compound **IIIa**

Run no.	Catalyst amount, g	Time, min	Yield, %
1	–	180	52
2	0.01	30	83
3	0.03	5	96
4	0.05	5	94

(500 MHz, $CDCl_3$), δ; ppm: 28.47, 30.44, 32.97, 33.36, 42.00, 116.79, 127.45, 129.19, 129.52, 145.25, 164.47, 193.22. IR (KBr), ν, cm^{-1}: 3014, 2873, 1667, 1624, 1510, 1360, 1215.

3,4,6,7-tetrahydro-3,3,6,6-tetramethyl-9-phenyl-2*H*-xanthene-1,8(-5*H*,9*H*)-dione (IIIb). White solid; mp: 202–203°C; ^{1}H NMR (500 MHz, $CDCl_3$), δ, ppm: 1.03 s (6H); 1.14 s (6H); 2.24 q (*J* = 15.70 Hz, 4H); 2.50 s (4H); 4.79 s (^{1}H); 7.24 m (5H). ^{13}C NMR (500 MHz, $CDCl_3$), δ, ppm: 27.29, 29.30, 31.47, 32.28, 40.84, 50.69, 115.26, 128.23, 129.78, 132.03, 142.71, 162.44, 196.00. IR (KBr), ν, cm^{-1}: 3019, 2964, 1667, 1625, 1464, 1215.

3,4,6,7-tetrahydro-3,3,6,6-tetramethyl-9-(4-nitrophenyl)-2*H*-xanthene-1,8-(5*H*,9*H*)-dione (IIIc). White solid; mp: 220–222°C; ^{1}H NMR (500 MHz, $CDCl_3$), δ, ppm: 1.15 s (6H), 1.28 s (6H), 2.35–2.54 m (8H), 5.58 s (^{1}H), 7.29 d (*J* = 8.8 Hz, 2H), 8.17 d (*J* = 8.8 Hz, 2H). ^{13}C NMR (125 MHz, $CDCl_3$), δ, ppm: 191.35, 147.0, 146.54, 130.9, 128.1, 123.9, 115.3, 47.4, 33.7, 31.9, 29.9, 27.9 IR (KBr), ν, cm^{-1}: 3100, 2920, 1680, 1600, 1540, 1510, 1340, 1200.

The other products were characterized by comparison of their spectroscopic and physical data with those of samples synthesized by reported procedures.

Computational details. All molecular structures were completely optimized at the B3LYP level of theory along with standard 6-31G(d) basis set. Harmonic vibration frequencies were calculated for all optimized structures to prove that true stationary points had been found. The gauge-independent atomic orbital (GIAO) NMR calculations were carried out at the B3LYP level using 6-31G(d) basis set. To study the aromaticity of the hetrocycles, the NICS at the center of all rings was calculated using the gauge independent atomic orbital (GIAO) method at the B3LYP level

Table 2. Synthesis of xanthenes using TCT

Run no.	Aldehyde	Time, min	Yield, %[a,b]	mp (observed)	mp (reported)	References
1	4-Methoxybenzaldehyde	5	96	242–243	242–243	[17]
2	Benzaldehyde	6	94	202–203	204–206	[17]
3	4-Nitrobenzaldehyde	2	98	220–222	221–223	[17]
4	4-Chlorobenzaldehyde	2	93	231–233	229–230	[17]
5	4-Methylbenzaldehyde	5	92	210–212	210–211	[17]
6	3-Nitrobenzaldehyde	3	97	171–173	170–172	[17]
7	2-Nitrobenzaldehyde	4	92	250–251	248–249	[17]
8	4-Hydroxybenzaldehyde	3	95	248–249	247–248	[17]
9	2-Chlorobenzaldehyde	5	90	225–226	225–227	[17]
10	2-Bromobenzaldehyde	5	91	225–227	226–229	[17]
11	4-Fluorobenzaldehyde	3	93	222–224	–	[17]

[a] Isolated yield. [b] The products were characterized by comparison of their spectroscopic and physical data with those of samples synthesized by published.

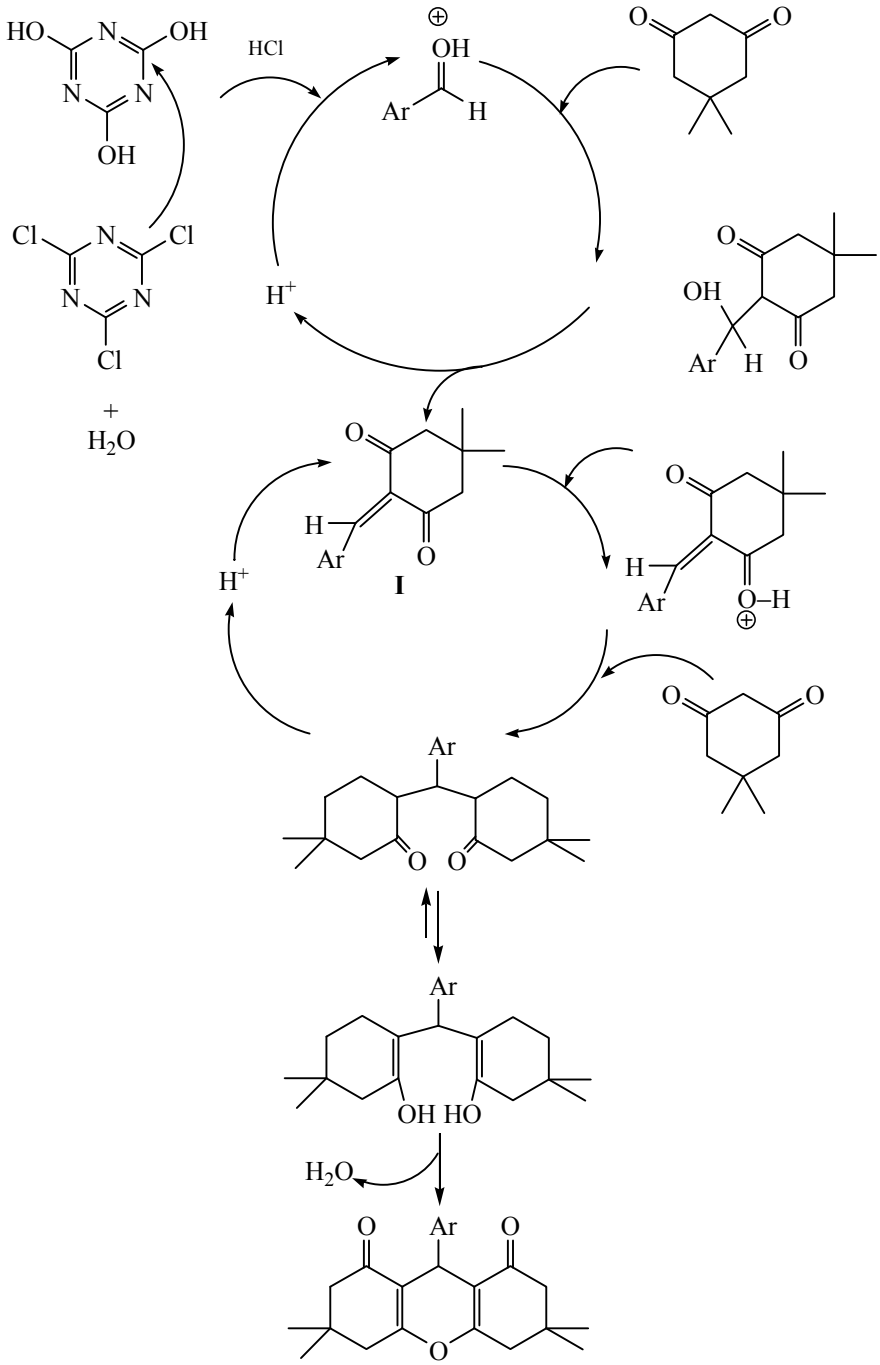

Scheme 2. Proposed mechanism of the TCT catalyzed synthesis of xanthenes.

using 6-31G(d) basis set. Calculations of geometry optimizations, vibration frequencies, and NMR parameters were carried out with GAUSSIAN 98 program [12].

RESULTS AND DISCUSSION

Recent developments in the xanthes chemistry and our continued interest in the development of an efficient and environmentally friendly procedure for the synthesis of pharmaceutical compounds [13–16] prompted us to synthesize of derivatives of xanthenes and to calculate the FT-IR, ^{1}H, and ^{13}C NMR spectra of selected compounds at the B3LYP level.

Initially, the optimization of catalyst amount to use in the synthesis of compound **IIIa** was performed

IIIa **IIIb** **IIIc**

Fig. 1. Geometry optimization of **IIIa–IIIc**.

(Table 1). The optimized amount of TCT to carry out this reaction is 0.03 g. The higher amount of TCT does not have any significamt effect on the reaction yield and time.

With the best catalyst in hand, several aromatic aldehydes were converted to correspounding xanthenes by the treatment with two equivalents of dimedones. The results are summerized in Table 2.

The possible mechanism of the synthesis of compounds **III** in the presence of TCT as a catalyst is shown in Scheme 2. On the basis of this mechanism, TCT catalyzes this reaction by conversion itself to HCl in situ and activating the aldehyde by making the carbonyl group susceptible to the nucleophilic attack by dimedone followed by the nucleophilic attack of the second molecule of dimedone on the α,β-unsaturated compound in Micheal addition reaction, enolization and dehydration giving product **III** as a result.

The geometries were optimized at the B3LYP level of theory with standard 6-31G(d) basis set as shown in Fig. 1. The harmonic vibration frequencies were calculated by this method and the results were compared with experimental FTIR spectrum. The most widely used technique for calculating NMR shielding tensors is the GIAO (Gauge Including Atomic Orbital) method. This method was used for calculating ^{1}H NMR and ^{13}C NMR chemical shifts at the B3LYP/6-31G(d) level. All the calculations were carried out with the Gaussian 03 software.

The structure and the scheme of atoms numbering in **IIIa–IIIc** are shown in Fig. 2.

Evaluation of data on bond distances, bond angles, and dihederal angles indicates the presence of resonance in pyran rings, since (a) the bond distances C–O in pyran rings are shorter than the standard value (C–O 1.43 Å) and (b) the bond angles C–O–C in pyran rings correspond to sp^2-hybridized bond angles (120°) as shown in Table 3.

The observed and calculated frequencies using DFT B3LYP/6-31G and probable assignments for **IIIa–IIIc** are summarized in Table 4. The C=C stretching bands appear at 1464–1625 cm^{-1} in the infrared spectrum. The bands occurring in the IR spectra at 1215 and 1360, 1215 and 1200 cm^{-1} in **IIIa–IIIc**, respectively are assigned to the C–O stretching vibrations. The C=O stretching bands are observed at 1667, 1667, and 1680 cm^{-1} in **IIIa–IIIc**, respectively.

The aromatic C–H stretching vibrations in **IIIa–IIIc** are observed at 3014, 3019, and 3100 cm^{-1}, respectively. The asymmetric and symmetric stretching vibrations of the nitro group are the most intense bands of the spectrum. The frequencies observed at 1510 cm^{-1} in the infrared spectrum are assigned to the $-NO_2$ asymmetric stretching modes of **IIIc**. The very strong symmetric stretching vibration of nitro group of the compound is assigned to the wave number 1340 cm^{-1} in the infrared spectra. The correction factors used to correlate the experimentally observed and theoretically computed frequencies for each vibration mode of **IIIa–**

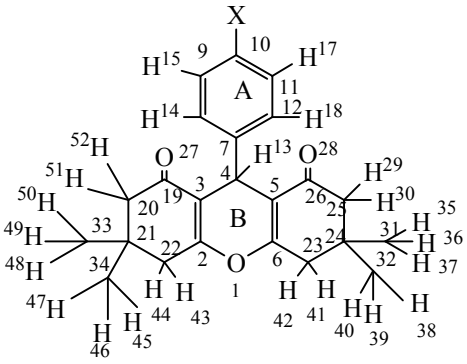

IIIa, X = OCH_3; **IIIb**, X = H; **IIIc**, X = NO_2;.

Fig. 2. Structure and atom numbering of **IIIa–IIIc.**

Table 3. Selected structural parameters calculated for **IIIa–IIIc** by DFT/B3LYP method with a 6-31G basis sets

Parameter	**IIIa**	**IIIb**	**IIIc**	Parameter	**IIIa**	**IIIb**	**IIIc**
Bond length				Bond angle			
$O^1–C^2$	1.3764	1.3764	1.3761	$C^2–O–C^6$	118.1703	118.1243	118.2373
$C^2–C^3$	1.3764	1.3764	1.3764	$C^5–C^4–C^7$	111.7056	111.5515	111.2752
$C^3–C^{19}$	1.4323	1.4671	1.4135	$C^5–C^4–H^{13}$	107.9273	108.0078	108.1880
$C^3–C^4$,	1.5237	1.5237	1.5234	$C^7–C^4–H^{13}$	107.2043	107.3702	107.3716
$C^4–C^5$	1.5237	1.5236	1.5234	$C^4–C^7–C^8$	121.2660	121.0132	120.9553
$C^4–C^7$	1.5377	1.5382	1.5373				
$C^4–H^{13}$	1.0930	1.0927	1.0925	Dihederal angle			
$C^5–C^6$	1.3764	1.3764	1.3764				
$C^7–C^8$	1.3996	1.3967	1.3984				
$C^8–C^9$	1.3881	1.3949	1.3909	$C^4–C^7–C^8–H^{14}$	0.0004	–0.006	0.0000
				$C^4–C^7–C^{12}–H^{18}$	0.0003	0.0031	0.0002
				$C^5–C^4–C^7–C^8$	–118.0281	–118.1448	–118.2126
$C^{19}–O^{27}$	1.2345	1.2453	1.2146	$C^5–C^4–C^7–C^{12}$	61.9711	61.8501	61.787
				$H^{13}–C^4–C^7–C^8$	0.0108	0.0071	0.0027

Table 4. Observed FTIR and frequencies calculated using B3LYP/6-31G(d) force field

Assignment	**IIIa**		**IIIb**		**IIIc**	
	calculated	experimental	calculated	experimental	calculated	experimental
ν(C–O)	1213.65	1215	1213.13	1215	1213.55	1200
ν(C–O)	1378.89	1360	–	–	–	–
$ν(NO_2)$	–	–	–	–	1366.06	1340
$ν(NO_2)$	–	–	–	–	1550.30	1510
ν(C=C)	1540.00	1510	1450.3	1464	1573.07	1540
ν(C=C)	1648.60	1624	1710.77	1625	1712.05	1600
ν(C=O)	1710.56	1667	1732.14	1667	1732.22	1680
ν(C–H) aliphatic	2999.45	2873	3017.26	2964	3009.85	2920
ν(C–H) aromatic	3016.85	3014	3089.13	3019	3095.37	3100

IIIc under DFT-B3LYP method are similar. The linear regression between the experimental and theoretical wave numbers of **IIIa–IIIc** are shown in Figs. 3 and 4. Thus, vibration frequencies calculated by using the B3LYP functional with 6-31G basis sets can be utilized to eliminate the uncertainties in the fundamental assignments in infrared vibration spectra.

The ^1H and ^{13}C theoretical and experimental chemical shifts, isotropic shielding tensors, and assignments of signals in the NMR spectra of **IIIa–IIIc** are presented in Tables 5 and 6, respectively. Aromatic carbons give signals in overlapped areas of the spectrum, with chemical shift values from 100 to 150 ppm in ^{13}C NMR, and 6–8.5 ppm in ^1H NMR spectra of **IIIa–IIIc**.

Due to the influence of electronegative atom, the chemical shift value of C^2 in **IIIa–IIIc** differ significantly in the shift positions, and the corresponding values of chemical shifts related to C^2 are 163.42 in **IIIa**, 162.44 in **IIIb**, and 164.53 ppm in **IIIc**, respectively. A downfield shift is observed for C^2 compared with C^3 in **IIIa–IIIc**. That is due to the mesomeric effect between $C^2–C^3–C^{19}–O^{27}$. The calculated and experimental chemical shift values given

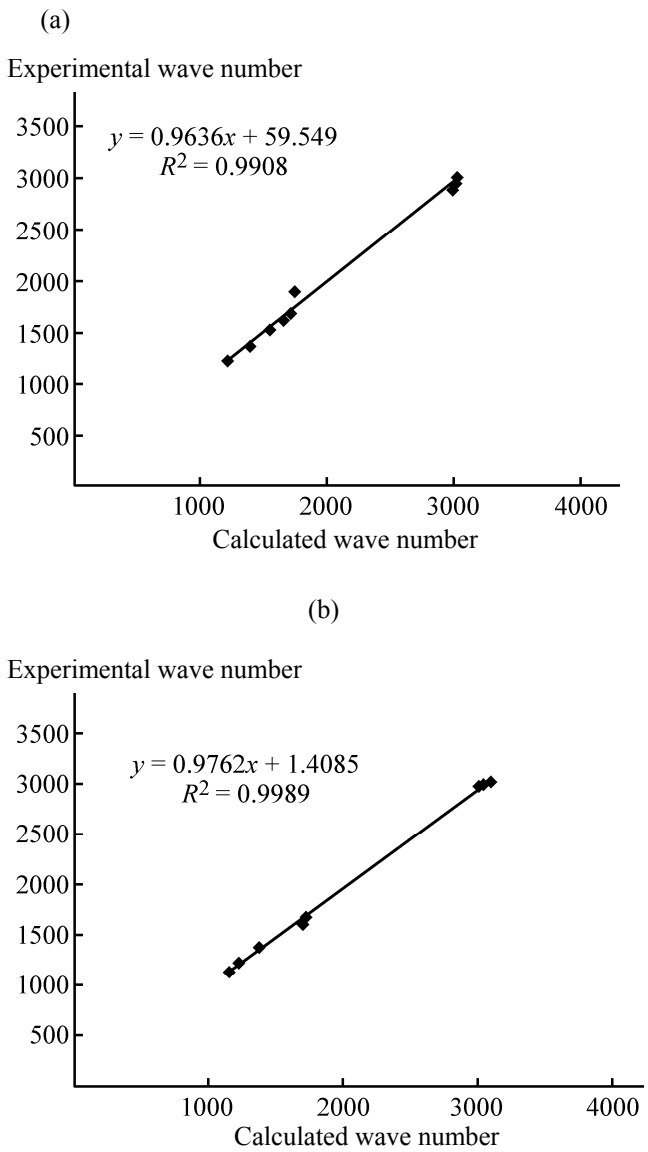

Fig. 3. A plot of correlation between experimental and theoretical IR spectra of (a) **IIIa** and (b) **IIIb** at the B3LYP/6-31G(d) level.

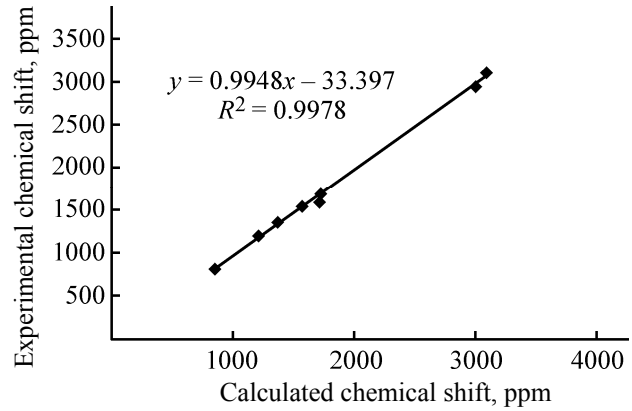

Fig. 4. A plot of correlation between experimental and theoretical IR spectrum of **IIIc** at the B3LYP/6-31G(d) level.

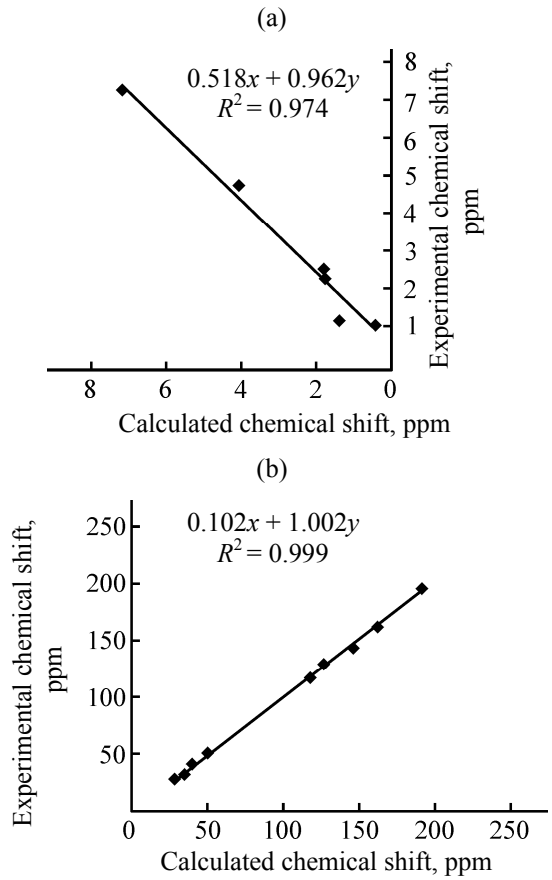

Fig. 5. A plot of correlation between experimental and theoretical (a) ^{1}H NMR and (b) ^{13}C NMR chemical shifts of **IIIa** calculated at the B3LYP/6-31G(d) level.

in Tables 5 and 6 show a good agreement. The linear regressions of the experimental and theoretical ^{1}H and ^{13}C NMR Chemical shifts of **IIIa**–**IIIc** are presented in Figs. 5–7.

Aromaticity is a central concept in explaining the structure, stability, and reactivity of certain molecules. It is commonly explained by the ring current theory that attributes the unique properties shared by aromatic molecules to a special electron delocalization in which the geometry allows the electrons a cyclic path for delocalization. NICS has been used as a reliable criterion of aromaticity since it has been proposed by Schleyer et al. in 1996.

According to the definition of NICS, which has been explained in the introduction part, the more

Table 5. Experimental and calculated ^{1}H NMR isotropic chemical shifts (ppm) with respect to TMS in the spectra of **IIIa–IIIc**

Assignment	**IIIa**		**IIIb**		**IIIc**	
	calculated	experimental	calculated	experimental	calculated	experimental
H^{50}, H^{49}, H^{48}	0.38	0.99	0.38	1.03	0.27	1.15
H^{47}, H^{46}, H^{45}	1.37	1.1	1.36	1.14	0.45	1.28
H^{44}, H^{43}	1.71	2.2	1.77	2.5 0	1.84	2.45
H^{51}, H^{52}	2.95	3.73	1.72	2.24	2.34	2.94
X^{16}	1.77	2.45	7.16	7.24	–	–
H^{13}	3.99	4.7 0	4.06	4.79	4.13	4.58
H^{17}	6.28	6.73	7.16	7.24	7.7	8.17
H^{18}	7.07	7.18	7.16	7.24	7.36	7.29

Table 6. Experimental and calculated ^{13}C NMR isotropic chemical shifts (ppm) with respect to TMS in the spectra of **IIIa–IIIc**

Assignment	**IIIa**		**IIIb**		**IIIc**	
	calculated	experimental	calculated	experimental	calculated	experimental
C^{33}	28.02	28.47	27.81	27.29	28.23	27.90
C^{21}	32.45	30.44	28.04	29.30	28.40	29.90
C^{22}	32.82	32.97	32.09	31.47	33.44	31.90
C^{4}	34.08	33.36	32.59	32.28	34.33	33.70
C^{20}	39.53	42.00	39.62	40.84	48.98	47.40
X^{16}	–	–	49.65	50.69	–	–
C^{3}	118.32	116.79	117.46	115.26	117.51	115.3
C^{11}	127.63	129.52	128.02	128.23	123.76	123.92
C^{12}	127.46	129.19	128.48	129.78	127.74	128.07
C^{7}	148.03	145.25	134.44	132.03	148.56	146.99
C^{10}	127.45	127.51	141.65	142.71	135.07	130.9
C^{2}	164.47	163.42	164.73	162.44	168.23	164.53
C^{19}	193.22	196.66	193.25	196.01	194.70	191.35

Table 7. Data for NICS calculation of **IIIa–IIIc**

Comp. no.	Ring	$NICS^{0}$	$NICS^{0.5}$	$NICS^{1}$
IIIa	A	–9.1716	–10.1449	–9.8130
	B	0.4442	–1.4045	–2.4810
IIIb	A	–8.4391	–10.0818	–10.3662
	B	0.8206	–0.9743	–1.7438
IIIc	A	–9.1781	–10.5063	–10.2512
	B	1.0328	–0.6805	–1.3901

negative the value of NICS the more aromatic is the molecule. The calculated NICSs of **IIIa–IIIc** are listed in Table 7. Comparison of the NICSs of ring A with that of ring B indicates that all of rings A are more aromatic than rings B.

The NICS calculated at 0, 0.5, and 1 Å indicates that the data will increase as the result of increasing distances from the centers of rings.

On the other hand, we found B ring has negative calculated $NICS^{1}$ and is relatively stable. We realize it has a homoaromatic structure as shown in Fig. 8.

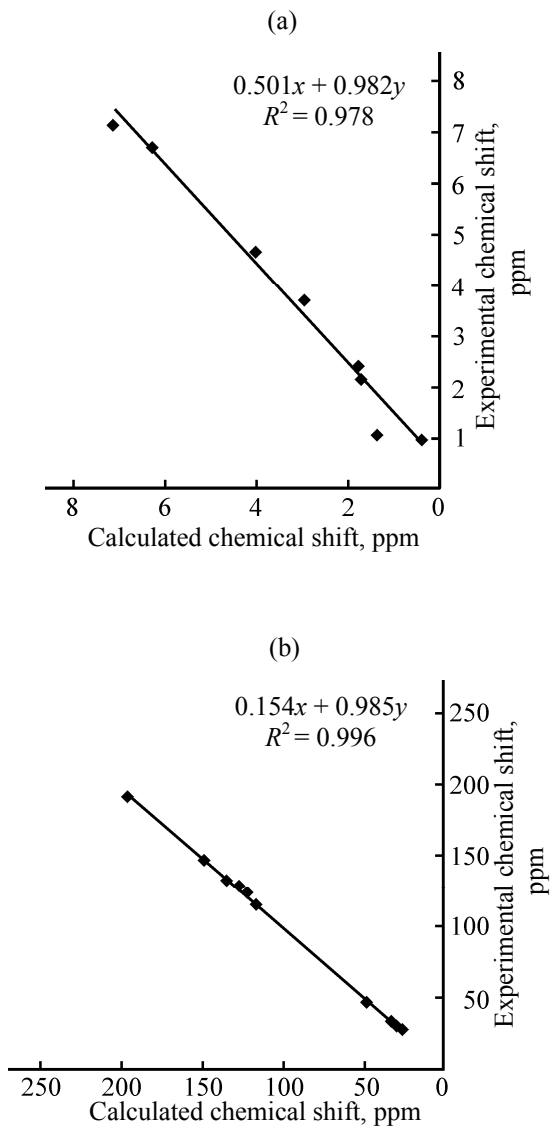

Fig. 6. A plot of correlation between experimental and theoretical (a) ^{1}H NMR and (b) ^{13}C NMR chemical shifts of **IIIb** calculated at the B3LYP/6-31G(d) level.

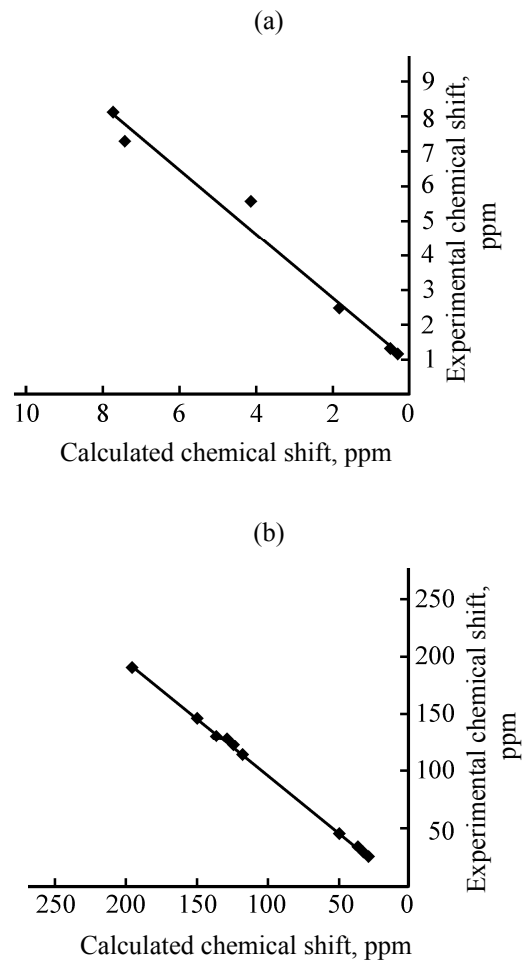

Fig. 7. A plot of correlation between experimental and theoretical (a) ^{1}H NMR and (b) ^{13}C NMR chemical shifts of **IIIc** calculated at the B3LYP/6-31G(d) level.

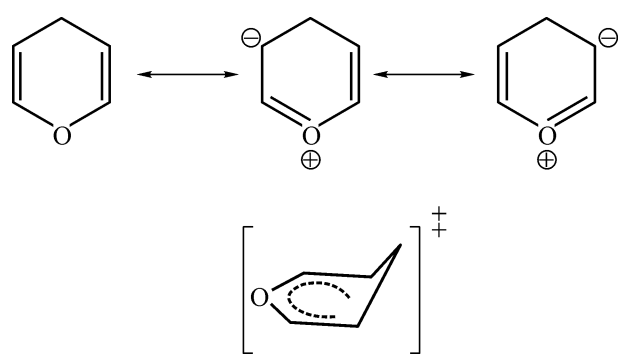

Fig. 8. Representation of homoaromaticity in xanthene ring.

CONCLUSIONS

The geometries of **IIIa–IIIc** were optimized with DFT-B3LYP using 6–31G basis sets. The selected molecular structural parameters of the optimized geometries of the compounds have been obtained from DFT calculations. The vibration frequencies of the fundamental modes of the compound have been precisely assigned and analyzed and the theoretical results were compared with the experimental vibrations. ^{1}H and ^{13}C NMR isotropic chemical shifts were calculated and the assignments made were compared with the experimental values. Thus the present investigation provides complete vibration assignments, structural information, and chemical shifts of the compounds. Finally, we present the calculated NICS values for all molecules

and discuss the change in their aromaticity associated with the structural modifications. The calculated NICS indicate that the xanthene ring is essentially homoaromatic with NICS values falling within the range from –1 to –2 ppm.

ACKNOWLEDGMENTS

We thank the Research Committee of Islamic Azad University of Rasht Branch for partial support given to this study.

REFERENCES

1. Sadeghi, B., Hassanabadi, A., and Taghvatalab, E., *J. Chemical Research*, 2003, vol. 35, no. 13, pp. 707–708.
2. Banerjee, A. and Mukherjee, A.K., *Biotech. Histochem.*, 1981, vol. 56, no. 2, pp. 83–85.
3. Callan, J.F., De Silva, P., and Magri, D.C., *Tetrahedron*, 2005, vol. 61, no. 36, pp. 8551–8588.
4. Chibale, K., Visser, M., Schalkwyk, D., Smith, P.J., Saravanamuthu, A., and Fairlamb, A.H., *Tetrahedron*, 2003, vol. 59, no. 13, pp. 2289–2296.
5. Knight, G.G. and Stephens, T., *Biochem. J.*, 1989, vol. 258, no. 3, pp. 683–687.
6. Ion, R.M., Wiktorowicz, K., Planner, A., and Frackowiak, D., *Acta Biochimica Polonica*, 1998, vol. 45, no. 3, pp. 833–845.
7. Koch, W. and Holthausen, M.C*., A Chemist's Guide to Density Functional Theory*, 2 ed., Weinheim: Wiley-VCH Verlag Gmbh, 2001.
8. Kohn, W., Becke, A.D., and Parr, R.G., *J. Phys. Chem.*, 1996, vol. 100, no. 31, pp. 12974–12980.
9. Lee, Ch., Yang, W., and Parr, R.G., *Phys. Rev. B*, 1988, vol. 37, no. 2, pp. 785–789.
10. Zhao, Y., Gonzalez-Garcia, N., and Truhlar, D.G., *J. Phys. Chem. A*, 2005, vol. 109, no. 9, pp. 2012–2018.
11. Schleyer, P.V.R., *Chem. Rev.,* 2001, vol.101, no. 5, pp. 1115–1118.
12. Frisch, M.J., Trucks, G.W., Schlegel, H.B., Scuseria, G.E., Robb, M.A., Cheeseman, J.R., Montgomery, J.A., Vreven, T., Kudin, K.N., Burant, J.C., Millam, J.M., Iyengar, S.S., Tomasi, J., Barone, V., Mennucci, B., Cossi, M., Scalmani, G., Rega, N., Petersson, G.A., Nakatsuji, H., Hada, M., Ehara, M., Toyota, K., Fukuda, R., Hasegawa, J., Ishida, M., Nakajima, T., Honda, Y., Kitao, O., Nakai, H., Klene, M., Li, X., Knox, J.E., Hratchian, H.P., Cross, J.B., Adamo, C., Jaramillo, J., Gomperts, R., Stratmann, R.E., Yazyev , O., Austin, A.J., Cammi, R., Pomelli, C., Ochterski, J.W., Ayala, P.Y., Morokuma, K., Voth, G.A., Salvador, P., Dannenberg, J.J., Zakrzewski, V.G., Dapprich, S., Daniels, A.D., Strain, M.C., Farkas, D.K. Malick, A.D. Rabuck, K. Raghavachari, J.B., Foresman, J.V., Ortiz, Q., Cui, A.G., Baboul, S., Clifford, J., Cioslowski, O., Stefanov, B.B., Liu, G., Liashenko, A., Komaromi, P.I., Martin, R.L., Fox, D.J., Keith, T., Al-Laham, M.A., Peng, C.Y., Nanayakkara, A., Challacombe, M., Gill, P.M.W., Johnson, B., Chen, W., Wong, M.W., Gonzalez, C., and Pople, J.A., *Gaussian03,* Revision B.03, Gaussian, Inc., Pittsburgh, PA, 2003.
13. Nikpassand, M., Mamaghani, M., Tabatabaeian, K., and Kupaei, M., *Molecular Diversity*, 2009, vol. 13, no. 3, pp. 389–393.
14. Zare, L. and Nikpassand, M., *Chinese Chem. Lett.,* 2011, vol. 22, no. 5, p. 531.
15. Nikpassand, M., Zare, L., and Saberi, M., *Monat. fur Chimie*, 2012, vol. 143, no.2 , p. 289.
16. Nikpassand, M., Zare, L., and Shafaati, T., *Chinese J. Chem.*, 2012, vol. 30, no. 3, pp. 604–608.
17. Li, J.J., Tao, X.Y., and Zhang, Z.H., *Phosphor. Sulf. Silicon Rel. Elem.,* 2008, vol. 183, no. 7, pp. 1672–1678.